A Triple Origin for the Heavy and Low-spin Binary Black Holes Detected by LIGO/VIRGO

Carl L. Rodriguez[1,3] and Fabio Antonini[2]
[1] MIT-Kavli Institute for Astrophysics and Space Research, 77 Massachusetts Avenue, 37-664H, Cambridge, MA 02139, USA
[2] Astrophysics Research Group, Faculty of Engineering and Physical Sciences, University of Surrey, Guildford, Surrey GU2 7XH, UK

Abstract

We explore the masses, merger rates, eccentricities, and spins for field binary black holes (BHs) driven to merger by a third companion through the Lidov–Kozai mechanism. Using a population synthesis approach, we model the creation of stellar-mass BH triples across a range of different initial conditions and stellar metallicities. We find that the production of triple-mediated mergers is enhanced at low metallicities by a factor of ~100 due to the lower BH natal kicks and reduced stellar mass loss. These triples naturally yield heavy binary BHs with near-zero effective spins, consistent with most of the mergers observed to date. This process produces a merger rate of between 2 and 25 $\text{Gpc}^{-3} \text{yr}^{-1}$ in the local universe, suggesting that the Lidov–Kozai mechanism can potentially explain all of the low-spin, heavy BH mergers observed by Advanced LIGO/Virgo. Finally, we show that triples admit a unique eccentricity and spin distribution that will allow this model to be tested in the near future.

Key words: gravitational waves – relativistic processes – stars: black holes

1. Introduction

With the detection of five binary black hole (BH) mergers and one binary BH (BBH) candidate (Abbott et al. 2016b, 2016c, 2017a, 2017b, 2017c), Advanced LIGO and Advanced Virgo will soon begin providing entire catalogs of BBH mergers. Even before the detection of GW150914, the first BBH merger, many different formation scenarios for BBHs had been proposed in the literature. These include formation from isolated binaries, either through a common-envelope phase (e.g., Belczynski et al. 2002, 2010, 2016; Podsiadlowski et al. 2003; Voss & Tauris 2003; Sadowski et al. 2008; Dominik et al. 2012, 2015, 2013) or through chemically homogeneous evolution via rapid rotation (e.g., De Mink & Mandel 2016; Mandel & De Mink 2016; Marchant et al. 2016), and dynamical formation in dense star clusters such as open clusters (e.g., Portegies Zwart & McMillan 2000; Banerjee et al. 2010; Ziosi et al. 2014; Banerjee 2017), globular clusters (e.g., Portegies Zwart & McMillan 2000; O'Leary et al. 2006, 2007; Moody & Sigurdsson 2009; Downing et al. 2010, 2011; Tanikawa 2013; Bae et al. 2014; Rodriguez et al. 2015, 2016a, 2016b, 2018; Askar et al. 2016; Giesler et al. 2018), or galactic nuclei (e.g., Miller & Lauburg 2009; O'Leary et al. 2009; Antonini & Perets 2012; Antonini & Rasio 2016; Bartos et al. 2017; VanLandingham et al. 2016; Petrovich & Antonini 2017; Stone et al. 2017; Hoang et al. 2018; Leigh et al. 2018). Despite their vastly different physical mechanisms, each of these formation channels has been invoked to solve the same problem: getting two BHs sufficiently close that the emission of gravitational waves (GWs) will lead them to merge.

To solve this problem, Silsbee & Tremaine (2017) and Antonini et al. (2017) proposed an alternative solution that invokes the secular interaction of a BBH with a third distant companion in the field of a galaxy. This third object can, at an appropriate separation and inclination, induce highly eccentric oscillations in the BBH, which will in turn promote a rapid merger of the binary through GW emission. This application of

the mechanism of Lidov (1962) and Kozai (1962) (LK) (see Naoz 2016, for a review) provides a natural, purely dynamical mechanism to drive BBHs to merge in the field of a galaxy without having to invoke the complicated and poorly constrained physics of common-envelope evolution. Despite the high multiplicity of triple systems around massive binaries (~60%, Sana et al. 2014), the contribution of stellar triples to the BBH merger rate remains minimally explored.

Furthermore, it has recently been shown (Antonini et al. 2018; Liu & Lai 2017, 2018) that the precession of the intrinsic spins of the BHs about the orbital angular momentum of the binary can produce significant misalignment between the orbital and spin angular momenta of merging BBHs from the LK channel. In Antonini et al. (2018), we showed that the spin evolution of a BBH during LK oscillations naturally leads to effective spins near zero, consistent with many of the LIGO/Virgo detections to date. Given that the spins of merging BBHs have been proposed as a promising way to discriminate between formation channels (Gerosa et al. 2013; Rodriguez et al. 2016c; Farr et al. 2017, 2018; Vitale et al. 2017), understanding the spin dynamics of any given formation channel is necessary to understand its contribution to the GW landscape.

In this paper, we explore BBH mergers from binaries driven to merger by the LK effect in galactic fields. We evolve a set of stellar triples to provide a realistic population of stellar-mass BH triples, which are in turn integrated using the secular LK equations including the relativistic spin–orbit (SO) and spin–spin (SS) couplings from post-Newtonian (pN) theory. We find that at low metallicities the production of LK-driven mergers from stellar triples is significantly enhanced, largely due to the lower BH natal kicks and reduced mass lost to stellar winds. Combined with an integration over the cosmic star formation rate (SFR), this enhancement suggests a BH merger rate between 1 and 25 $\text{Gpc}^{-3} \text{yr}^{-1}$ in the local universe, competitive with other formation channels. These low-metallicity LK-driven mergers, with their large masses and near-zero effective
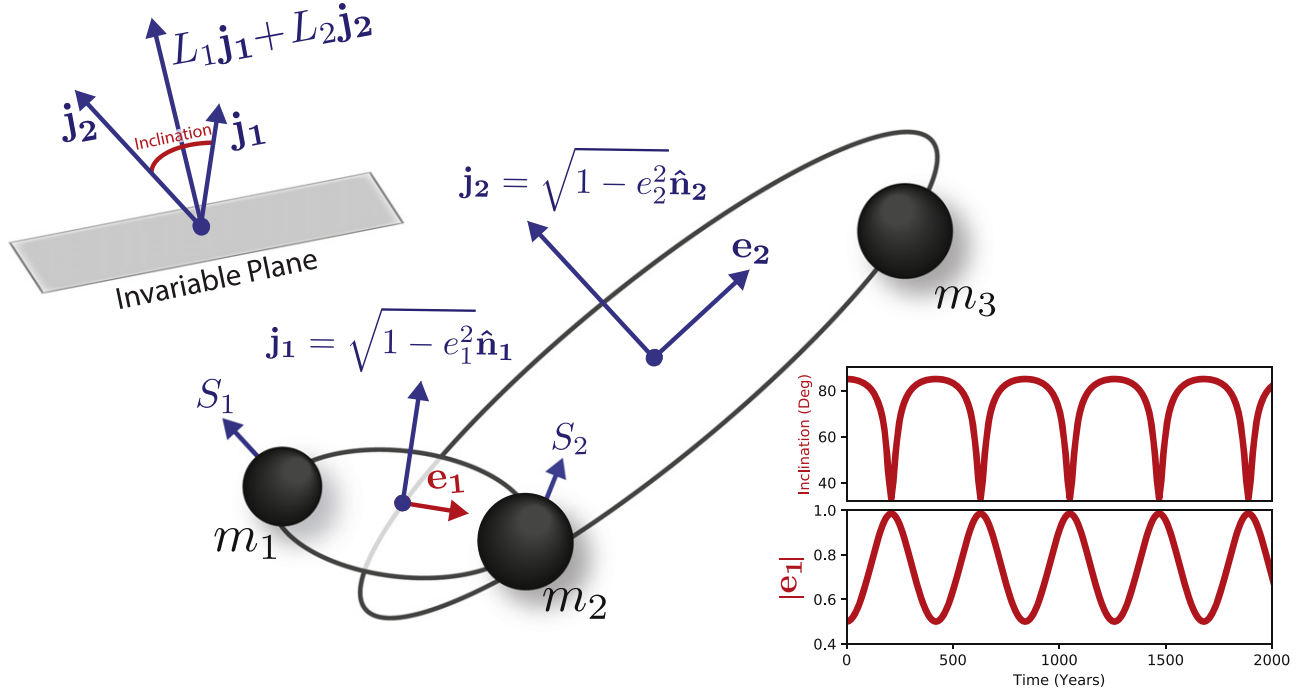
---

[3] Pappalardo Fellow.

Figure 1. An illustration of the general problem considered in this paper and the geometric formalism we use. For any triple system, the total angular momentum of the system is conserved (in the absence of GW emission) and defines a fixed "invariable plane" of the system. L_1 and L_2 define the circular angular momenta of each binary (e.g., $L_1 = \mu\sqrt{G(m_1 + m_2)a}$), while the dimensionless angular momentum (j_1 and j_2) and eccentricity (e_1 and e_2) vectors are used to define the orientation and orbital elements of the triple. The eccentricity of the inner binary (e_1) and the mutual inclination of the two binaries change during an LK oscillation, as the two binaries exchange angular momentum while precessing about the total angular momentum of the system. The plot shows several LK oscillations for a triple with $m_1 = m_2 = m_3 = 1\,M_\odot$, $a_1 = 1$ au, $a_2 = 10$ au, $e_2 = 0.2$, and an initial state of $e_1 = 0.5$ and $i = 85°$. S_1 and S_2 define the spin vectors of the inner BHs, which we assume do not directly couple to the outer binary.

spins, can easily explain all of the heavy, low-spin BBH mergers observed by LIGO/Virgo.

In Section 2, we re-derive the relativistic corrections to the binary motion arising from the precession of the pericenter and the lowest-order SO and SS terms, using a Hamiltonian formalism developed in Tremaine et al. (2009), Petrovich (2015), and Liu et al. (2015), and explore the resultant implications for the spin evolution. In Section 3, we describe the setup of our triple population synthesis technique, while in Section 4 we describe the features of our population of evolved BH triples. In Section 5, we show how the distribution of BH spins from merging triples (and in particular the distributions of the effective spins) naturally forms a population of mergers with near-zero effective spins, while in Section 6 we showcase various observable parameters from our BBH merger population (including the masses, eccentricities, and spins), and compute the merger rate of BH triples. Throughout this paper, we assume a ΛCDM cosmology with $h = 0.679$ and $\Omega_M = 0.3065$ (Ade et al. 2016), and that all BHs are born maximally spinning (although we relax this assumption in Section 6.1).

2. Secular Equations of Motion

We are interested in the long-term evolution of triple systems for which the relativistic contributions to the inner binary become significant. To set up our dynamical problem, we use the LK equations of motion to octupole order (Liu et al. 2015; Petrovich 2015) using the geometric formalism developed in Tremaine et al. (2009) and Correia et al. (2011). See Tremaine & Yavetz (2014) for a detailed explanation. In this formalism, the orientations of the binaries and their orbital elements are

described using the dimensionless angular momentum and Laplace–Runge–Lenz vectors, j and e, defined such that

$$j \equiv \sqrt{1 - e^2}\,\hat{n}$$
$$e \equiv e\hat{u}$$

where e is the eccentricity of the binary, e points in the direction of the binary pericenter, and j points along the orbital angular momentum of the binary. See Figure 1. We also define the scalar angular momentum for a circular binary

$$L \equiv \mu\sqrt{GMa}$$

such that $L \times j$ is the standard angular momentum vector, with $M \equiv m_1 + m_2$ and $\mu \equiv m_1 m_2 / M$ being the reduced mass of the binary.

The power of this formalism lies in the fact that the Poisson brackets of the angular momentum and eccentricity vectors can be expressed as

$$\{j_i, j_j\} = \frac{1}{L}\epsilon_{ijk}j_k$$
$$\{e_i, e_j\} = \frac{1}{L}\epsilon_{ijk}j_k$$
$$\{j_i, e_j\} = \frac{1}{L}\epsilon_{ijk}e_k \qquad (1)$$

where ϵ_{ijk} is the Levi–Civita symbol. It is then straightforward to show that, for any Hamiltonian H, the equations of motion

can be expressed as (Tremaine et al. 2009)

$$\frac{df}{dt} = \{f, H\}$$
$$= \{f, \boldsymbol{j}\}\, \boldsymbol{\nabla}_j H + \{f, \boldsymbol{e}\}\, \boldsymbol{\nabla}_e H$$

which, when combined with the Poisson brackets from Equations (1), yields

$$\frac{d\boldsymbol{j}}{dt} = \frac{1}{L}(\boldsymbol{e} \times \boldsymbol{\nabla}_e H + \boldsymbol{j} \times \boldsymbol{\nabla}_j H) \qquad (2)$$

$$\frac{d\boldsymbol{e}}{dt} = -\frac{1}{L}(\boldsymbol{j} \times \boldsymbol{\nabla}_e H + \boldsymbol{e} \times \boldsymbol{\nabla}_j H). \qquad (3)$$

To determine the orbital evolution of a system, all that remains is to specify the orbit-averaged Hamiltonian to be inserted into Equations (2) and (3).

For a non-spinning triple system, the LK Hamiltonian H_{LK} can be written as

$$H_{\mathrm{LK}} = H_1 + H_2 + H_{12} \qquad (4)$$

where H_1 and H_2 are the Keplerian Hamiltonians for the inner and outer binaries, and H_{12} is an interaction term between the two, often expressed as a series expansion in the instantaneous separation between the two binaries (Kozai 1962; Lidov 1962; Harrington 1968; Ford et al. 2000; Naoz et al. 2013). We use the geometric form of these equations developed in Petrovich (2015) and Liu et al. (2015), accurate up to the octupole order of the interaction term. See Equations (17)–(20) in Liu et al. (2015).

To account for the pN corrections to the Newtonian three-body problem, we can self-consistently add additional terms to the Hamiltonian, accounting for pericenter precession at first pN order (1pN), the evolution of the BH spins due to geodetic precession about $\boldsymbol{j}_1$ (1pN), the back-reaction on the orbit from Lense–Thirring precession (1.5pN, Damour & Schäer 1988), and the gravitomagnetic coupling between the two spins and the quadrupole–monopole interaction (2pN, Barker & O'Connell 1975; Damour 2001). The complete Hamiltonian then becomes

$$H = H_{\mathrm{LK}} + H_{\mathrm{1pN}} + H_{\mathrm{SO}} + H_{\mathrm{SS}} \qquad (5)$$

where the pN couplings between the orbit of the inner masses and their spins are given by (e.g., Damour & Schäer 1988; Buonanno et al. 2011)

$$H_{\mathrm{1pN}} = \frac{\mu}{c^2}\left[\frac{(3\mu/M - 1)\boldsymbol{p}_1^{\,4}}{8} - \frac{G\mu(\boldsymbol{p}_1 \cdot \hat{\boldsymbol{r}}_1)^2}{2r_1} \right.$$
$$\left. - \frac{(3 + \mu/M)GM\boldsymbol{p}_1^{\,2}}{2r_1} + \frac{(GM)^2}{2r_1^2}\right] \qquad (6)$$

$$H_{\mathrm{SO}} = \frac{2GL_1}{c^2|\boldsymbol{r}_1|^3}\boldsymbol{S}_{\mathrm{eff}} \cdot \boldsymbol{j}_1 \qquad (7)$$

$$H_{\mathrm{SS}} = \frac{G\mu}{2c^2M|\boldsymbol{r}_1|^3}[3(\boldsymbol{S}_0 \cdot \hat{\boldsymbol{n}}_1)^2 - \boldsymbol{S}_0^2] \qquad (8)$$

where $\boldsymbol{r}_1$ and $\boldsymbol{p}_1$ are the reduced positions and momenta of the inner binary, and where we introduce two new combinations of the BH spin vectors:

$$\boldsymbol{S}_{\mathrm{eff}} = \left(1 + \frac{3m_2}{4m_1}\right)\boldsymbol{S}_1 + \left(1 + \frac{3m_1}{4m_2}\right)\boldsymbol{S}_2$$

$$\boldsymbol{S}_0 = \left(1 + \frac{m_2}{m_1}\right)\boldsymbol{S}_1 + \left(1 + \frac{m_1}{m_2}\right)\boldsymbol{S}_2$$

where $\boldsymbol{S}_1$ and $\boldsymbol{S}_2$ correspond to the spin vectors of m_1 and m_2. These can also be written in terms of the dimensionless spin parameter χ as

$$\boldsymbol{S}_i = \chi_i \frac{Gm_i^2}{c}, \quad |\chi_i| \leqslant 1. \qquad (9)$$

Averaging each of these terms over an orbital period (see, e.g., Tremaine & Yavetz 2014), we can express the orbit-averaged contributions from each pN effect as

$$\langle H_{\mathrm{1pN}}\rangle = \frac{G^2M^2\mu}{8c^2a_1^2}\left[15 - \frac{\mu}{M} - \frac{24}{\sqrt{1 - e_1^2}}\right] \qquad (10)$$

$$\langle H_{\mathrm{SO}}\rangle = \frac{2GL_1}{c^2a_1^3(1 - e_1^2)^{3/2}}\boldsymbol{S}_{\mathrm{eff}} \cdot \boldsymbol{j}_1 \qquad (11)$$

$$\langle H_{\mathrm{SS}}\rangle = \frac{G\mu}{2c^2Ma_1^3(1 - e_1^2)^{3/2}}\left[\frac{1}{2}\boldsymbol{S}_0^2 - \frac{3}{2}(\boldsymbol{S}_0 \cdot \hat{\boldsymbol{n}}_1)^2\right]. \qquad (12)$$

To derive the equations of motion from Equations (10)–(12), we simply calculate the derivatives using Equations (2) and (3). For the contribution from $\langle H_{\mathrm{1pN}}\rangle$, we find

$$\frac{d\boldsymbol{e}_1}{dt}\bigg|_{\mathrm{1pN}} = \{\boldsymbol{e}_1, \langle H_{\mathrm{1pN}}\rangle\}$$

$$= -\frac{1}{L_1}[\{\boldsymbol{e}_1, \boldsymbol{e}_1\}\nabla_{e_1}\langle H_{\mathrm{1pN}}\rangle + \{\boldsymbol{e}_1, \boldsymbol{j}_1\}\nabla_{j_1}\langle H_{\mathrm{1pN}}\rangle]$$

$$= \frac{3(GM)^{3/2}}{c^2a_1^{5/2}(1 - e_1^2)^{3/2}}\boldsymbol{j}_1 \times \boldsymbol{e}_1$$
$$\qquad (13)$$

with $\boldsymbol{j}_1$ conserved at 1pN order prior to the inclusion of spin effects or GW emission. This is identical to the pericenter precession term found in the literature (Eggleton & Kiseleva-Eggleton 2001; Fabrycky & Tremaine 2007; Liu et al. 2015), but falls naturally out of the orbit-averaged vector formalism. We then consider the SO and SS terms. In addition to the Poisson brackets between $\boldsymbol{j}$ and $\boldsymbol{e}$, we introduce Poisson brackets for the spin vectors:

$$\{S_1^i, S_1^j\} = \epsilon_{ijk}S_1^i S_1^j$$
$$\{S_2^i, S_2^j\} = \epsilon_{ijk}S_2^i S_2^j$$
$$\{S_1^i, S_2^j\} = 0 \qquad (14)$$

with all other Poisson brackets ($\{S_1^i, j_1^j\}$, $\{S_1^i, e_1^j\}$, $\{S_1^i, j_2^j\}$, $\{S_1^i, e_2^j\}$, and their $1 \leftrightarrow 2$ equivalents) being zero. We can then explicitly write down the orbit-averaged equations of motion from $\langle H_{\mathrm{SO}}\rangle$ and $\langle H_{\mathrm{SS}}\rangle$:

$$\frac{d\boldsymbol{j}_1}{dt}\bigg|_{\mathrm{SO}} = \frac{2G}{c^2a_1^3(1 - e_1^2)^{3/2}}\boldsymbol{S}_{\mathrm{eff}} \times \boldsymbol{j}_1 \qquad (15)$$

$$\frac{d\boldsymbol{e}_1}{dt}\bigg|_{\mathrm{SO}} = \frac{2G}{c^2 a_1^3 (1-e_1^2)^{3/2}}[\boldsymbol{S}_{\mathrm{eff}} - 3(\boldsymbol{S}_{\mathrm{eff}} \cdot \hat{\boldsymbol{n}}_1)\hat{\boldsymbol{n}}_1] \times \boldsymbol{e}_1 \quad (16)$$

$$\frac{d\boldsymbol{S}_1}{dt}\bigg|_{\mathrm{SO}} = \frac{2G^{3/2}\mu M^{1/2}}{c^2 a_1^{5/2}(1-e_1^2)^{3/2}}\left(1 + \frac{3m_2}{4m_1}\right)\boldsymbol{j}_1 \times \boldsymbol{S}_1 \quad (17)$$

and similarly for $\boldsymbol{S}_2$. The SS terms can be derived in a similar fashion:

$$\frac{d\boldsymbol{j}_1}{dt}\bigg|_{\mathrm{SS}} = -\frac{3G^{1/2}}{2c^2 M^{3/2} a_1^{7/2}(1-e_1^2)^2}(\boldsymbol{S}_0 \cdot \hat{\boldsymbol{n}}_1)\boldsymbol{S}_0 \times \boldsymbol{j}_1 \quad (18)$$

$$\frac{d\boldsymbol{e}_1}{dt}\bigg|_{\mathrm{SS}} = \frac{3G^{1/2}}{4c^2 M^{3/2} a_1^{7/2}(1-e_1^2)^2}$$
$$\times [5(\boldsymbol{S}_0 \cdot \hat{\boldsymbol{n}}_1)^2\hat{\boldsymbol{n}}_1 - 2(\boldsymbol{S}_0 \cdot \hat{\boldsymbol{n}}_1)\boldsymbol{S}_0 - S_0^2\hat{\boldsymbol{n}}_1)] \times \boldsymbol{e}_1$$
$$(19)$$

$$\frac{d\boldsymbol{S}_1}{dt}\bigg|_{\mathrm{SS}} = \frac{G\mu}{2c^2 M a_1^3 (1-e_1^2)^{3/2}}\left(1 + \frac{m_2}{m_1}\right)$$
$$\times [\boldsymbol{S}_0 - 3(\boldsymbol{S}_0 \cdot \hat{\boldsymbol{n}}_1)\hat{\boldsymbol{n}}_1] \times \boldsymbol{S}_1 \quad (20)$$

and similarly for $\boldsymbol{S}_2$. Equations (13) and (15)–(20), combined with the octupole-order LK equations from Liu et al. (2015), give us the complete equations of motion for a triple with spinning inner components described by the Hamiltonian in Equation (5), and are fully consistent with previously derived results in the literature for isolated binaries (Barker & O'Connell 1975).

When defining the BH spins, we find it convenient to define the angles between the spins and the orbital angular momentum as

$$\theta_1 \equiv \cos^{-1}\left(\frac{\boldsymbol{S}_1 \cdot \boldsymbol{j}_1}{|\boldsymbol{S}_1 \cdot \boldsymbol{j}_1|}\right)$$

and similarly for θ_2. We also define the angle between the components of the spins lying in the orbital plane,

$$\Delta\phi \equiv \cos^{-1}\left(\frac{\boldsymbol{j}_1 \times \boldsymbol{S}_1}{|\boldsymbol{j}_1 \times \boldsymbol{S}_1|} \cdot \frac{\boldsymbol{j}_1 \times \boldsymbol{S}_2}{|\boldsymbol{j}_1 \times \boldsymbol{S}_2|}\right).$$

However, the spin parameter best constrained by the current generation of GW detectors is the effective binary spin (Ajith et al. 2011; Vitale et al. 2014; Pürrer et al. 2016), defined as the mass-weighted projection of the two spins onto the orbital angular momentum:

$$\chi_{\mathrm{eff}} \equiv \left(\frac{m_1\boldsymbol{\chi}_1 + m_2\boldsymbol{\chi}_2}{m_1 + m_2}\right) \cdot \hat{\boldsymbol{n}}_1. \quad (21)$$

In the following sections, we will primarily focus on χ_{eff} as the main spin observable of interest to Advanced LIGO/Virgo.

Since each of the above dynamical equation resembles an expression for simple precession (e.g., $\dot{\boldsymbol{u}} = \boldsymbol{\Omega} \times \boldsymbol{u}$), it is straightforward to write down the timescale associated with each effect as $t \approx \pi/|\boldsymbol{\Omega}|$. At 1pN order, the timescale for the precession of $\boldsymbol{e}_1$ about $\boldsymbol{j}_1$ (Equation (13), often referred to as pericenter, Schwarzschild, or apsidal precession) is

$$t_{1\mathrm{pN}} = \frac{\pi c^2 a_1^{5/2}(1-e_1^2)}{3(GM)^{3/2}}. \quad (22)$$

Also at 1pN order, the timescale for the precession of the spins $\boldsymbol{S}_1$ and $\boldsymbol{S}_2$ about $\boldsymbol{j}_1$ is

$$t_{S_1} = \frac{\pi c^2 a_1^{5/2}(1-e_1^2)}{2G^{3/2}\mu M^{1/2}}\left(1 + \frac{3m_2}{4m_1}\right)^{-1} \quad (23)$$

and similarly for $\boldsymbol{S}_2$. Note that, while SO effects are frequently referred to as 1.5pN order, the *simple precession of the spins about $\boldsymbol{j}_1$ is formally a 1pN effect*. This effect, often referred to as de Sitter or geodetic precession, is nothing more than the change in the angles arising from the parallel transport of the spins about the orbit. Similar timescales can be derived for the higher-order SO and SS effects. Although we do not write them down here, we note that the timescales from Equations (15)–(20) agree with results in the literature (e.g., Merritt 2013) in the limit of $\boldsymbol{S}_2 \to 0$. Additionally, we define the quadrupole timescale for a single LK oscillation of the triple as

$$t_{\mathrm{LK}} = \frac{m_1 + m_2}{\nu m_3}\left(\frac{a_2\sqrt{1-e_2^2}}{a_1}\right)^3 \quad (24)$$

where $\nu \equiv \sqrt{G(m_1 + m_2)/a_1^3}$ is the mean motion of the inner binary.

Finally, we add the dissipation in a_1 and e_1 from the emission of GWs. As writing down Hamiltonians for non-conservative processes requires special mathematical care, we instead simply add the known contributions from Peters (1964):

$$\left\langle\frac{da}{dt}\right\rangle = -\frac{64}{5}\frac{G^3 m_1 m_2(m_1 + m_2)}{c^5 a^3(1-e^2)^{7/2}}$$
$$\times \left(1 + \frac{73}{24}e^2 + \frac{37}{96}e^4\right) \quad (25)$$

$$\left\langle\frac{de}{dt}\right\rangle = -\frac{304}{15}e\frac{G^3 m_1 m_2(m_1 + m_2)}{c^5 a^4(1-e^2)^{5/2}}$$
$$\times \left(1 + \frac{121}{304}e^2\right). \quad (26)$$

During each integration timestep, we compute the change in a_1 from Equation (25), while the change in eccentricity is included in the geometric variables as

$$\frac{d\boldsymbol{e}_1}{dt}\bigg|_{\mathrm{GW}} = \left\langle\frac{de}{dt}\right\rangle\hat{\boldsymbol{e}}_1$$

$$\frac{d\boldsymbol{j}_1}{dt}\bigg|_{\mathrm{GW}} = -\left\langle\frac{de}{dt}\right\rangle\frac{e_1}{\sqrt{1-e_1^2}}\hat{\boldsymbol{n}}_1,$$

allowing us to self-consistently track the change in angular momentum from GW emission during our triple integration.

2.1. Secular Dynamics of Spinning Triples

The chaotic evolution of spins during the evolution of triple systems has been well described in the context of planetary systems (e.g., Storch et al. 2014; Liu et al. 2015; Storch & Lai 2015). In that case, the evolution of the spin vector can be classified by comparing the precession timescales of the orbital angular momentum of the binary (during an LK oscillation) to the precession of the spin vector about the total angular momentum of the inner binary (due to tidal forces). If the

precession rate of S_1 about j_1 is significantly longer than the precession of j_1 about the total angular momentum of the system, then the spins are expected to effectively precess about the total angular momentum, keeping a constant angle with respect to the invariable plane (the "non-adiabatic" case). For our problem, this would correspond to $t_{S_1} > t_{LK}$. On the other hand, if the precession of S_1 about j_1 is significantly faster than the precession of j_1 (i.e., $t_{S_1} < t_{LK}$), the spins are expected to adiabatically follow j_1, virtually oblivious to the presence of the third companion. The intermediate "trans-adiabatic" regime, in which $t_{S_1} \sim t_{LK}$, allows for chaotic evolution of the spins, and is thought to play an important role in the observed spins of many exo-planetary systems (Storch et al. 2014).

Although we might expect to observe a similar behavior for the spinning BH systems studied here, we now show that this is not the case. We define the adiabaticity parameter (with S_1 as the spin of the more massive BH) as

$$R \equiv \frac{t_{LK}}{t_{S_1}} \qquad (27)$$

such that any triple for which $R < 1$ is considered non-adiabatic, while those where $R > 1$ are considered adiabatic. While the LK timescale remains unchanged during the evolution of the triple (ignoring GW emission), the timescale for spin precession varies as $(1 - e_1^2)$, meaning that the spin timescale could decrease by several orders of magnitude over the course of a single LK oscillation. Thus, one might think that a triple can easily transit from the non-adiabatic to the adiabatic regime, where its brief moment in the trans-adiabatic regime can induce chaotic evolution in the spin vectors.

Unfortunately, the potential chaotic spin evolution is largely suppressed by a conspiracy of relativity (Antonini et al. 2018). Both the precession of S_1, S_2 about j_1 (Equation (23)) and the precession of the pericenter of the inner binary (Equation (22)) are formally 1pN order contributions, and both scale as $a_1^{5/2}(1 - e_1^2)$. However, it is well known that short-range forces between components of the inner binary—particularly pericenter precession—can quench LK oscillations in a hierarchical triple, since at a certain separation the inner binary will precess so rapidly that it decouples from the outer binary. Conceptually, this point can be thought of as the separation where the time for the inner binary to precess by π is shorter than the timescale to change j_1 by the order of itself. Thus, by setting $t_{1pN} = t_{LK}j_1$ we find the angular momentum below which LK oscillations are quenched by relativistic precession[4] (Antonini et al. 2018):

$$j_{GR} = \frac{3G}{\pi c^2} \frac{(m_1 + m_2)^2}{m_3} \left(\frac{a_2 j_2}{a_1} \right)^3 \frac{1}{a_1}. \qquad (29)$$

What Equation (29) describes is an angular momentum barrier that cannot be passed by systems that evolve from

$j_1 > j_{GR}$. Because the pericenter and spin precession terms enter at the same order in the pN expansion, we find that $R = 1$ near the barrier, implying that initially non-adiabatic systems ($R < 1$) cannot become adiabatic ($R > 1$) in the absence of GW dissipation. For the population we study in Section 4, roughly 99% of the BH triples begin their evolution in the non-adiabatic regime, with 87% of systems having $R < 0.1$ and 60% having $R < 0.01$. At the same time, any triple that may try to evolve into the trans-adiabatic regime is stopped by the angular momentum barrier. We conclude that any trans-adiabatic (and possibly chaotic) evolution of the SO orientation is suppressed. As such, while we might expect a wide range of SO misalignments from triples in the non-adiabatic regime, especially for cases where the eccentric LK mechanism can produce orbital flips of the system (e.g., Naoz et al. 2011), we do not expect to see truly chaotic evolution of the triple spins as one does for planetary systems.

2.2. GW Emission and Freezing the Spin Angles

At the peak of an LK oscillation, the eccentricity of the inner binary reaches its maximum, and the energy lost via GW emission can become important for the dynamical evolution of the triple. We can write the timescale for GW radiation as

$$t_{GW} = a \left| \frac{da}{dt} \right|^{-1} \qquad (30)$$

where the derivative is given by Equation (25). The value of the angular momentum where GW radiation dominates over the LK dynamics can be derived by setting $t_{GW} = t_{LK} j_1$, which gives

$$j_{GW} = \left(\frac{170 G m_1 m_2}{3 c^5 m_3} \frac{a_2^3 j_2^3}{a_1} \nu^3 \right)^{1/6}. \qquad (31)$$

For $j_1 \leqslant j_{GW}$ the inner binary effectively decouples from the third body, and the BBH merges as an isolated system.

Two situations are relevant here: (i) the 2.5pN terms dominate the evolution of the binary before the 1pN pericenter precession can affect the LK oscillations, and (ii) the 1pN terms become important before the 2.5pN terms and arrest the evolution of the triple.

In case (i), the inner binary "plunges" directly into the regime where GWs dominate its evolution during the maximum eccentricity phase of an LK oscillation. After this regime is reached, the evolutions of e_1 and a_1 are the same as in an isolated binary evolving under GW emission alone; this happens after approximately one LK cycle (starting from $e_1 \approx 0$) at the quadrupole level of approximation, or could take several LK cycles at the octupole level. We show an example of this type of evolution in the left panels of Figure 2. The inner binary in this case undergoes extreme ($e_1^{max} > 0.99999$) LK oscillations arising from the strong contribution of the octupole-order terms, including several flips of the inner orbit. In this strongly non-adiabatic case, the LK oscillations are several orders of magnitude faster than the spin precession timescale of the binary, and the spins remain essentially fixed while j_1 varies significantly right up to the merger of the inner binary.

In case (ii), when the precessional effect becomes important before the dissipative effects dominate, e_1 and the inclination experience damped oscillations, where the angular momentum

---

[4] An alternative criterion can be derived by requiring that pericenter precession becomes so strong at a certain separation that the fixed point of the LK problem no longer exists. This leads to the following condition for LK oscillations to be fully quenched by the 1pN pericenter precession (Blaes et al. 2002):

$$\left(\frac{a_2}{a_1} \right)^3 > \frac{3 c^2 m_3 a_1}{4 G (m_1 + m_2)^2} \left(\frac{1 - e_1^2}{1 - e_2^2} \right)^{3/2}. \qquad (28)$$

In the next sections, we use Equation (28) to classify systems that will be completely suppressed by pericenter precession, because it is a more conservative criterion than Equation (29).
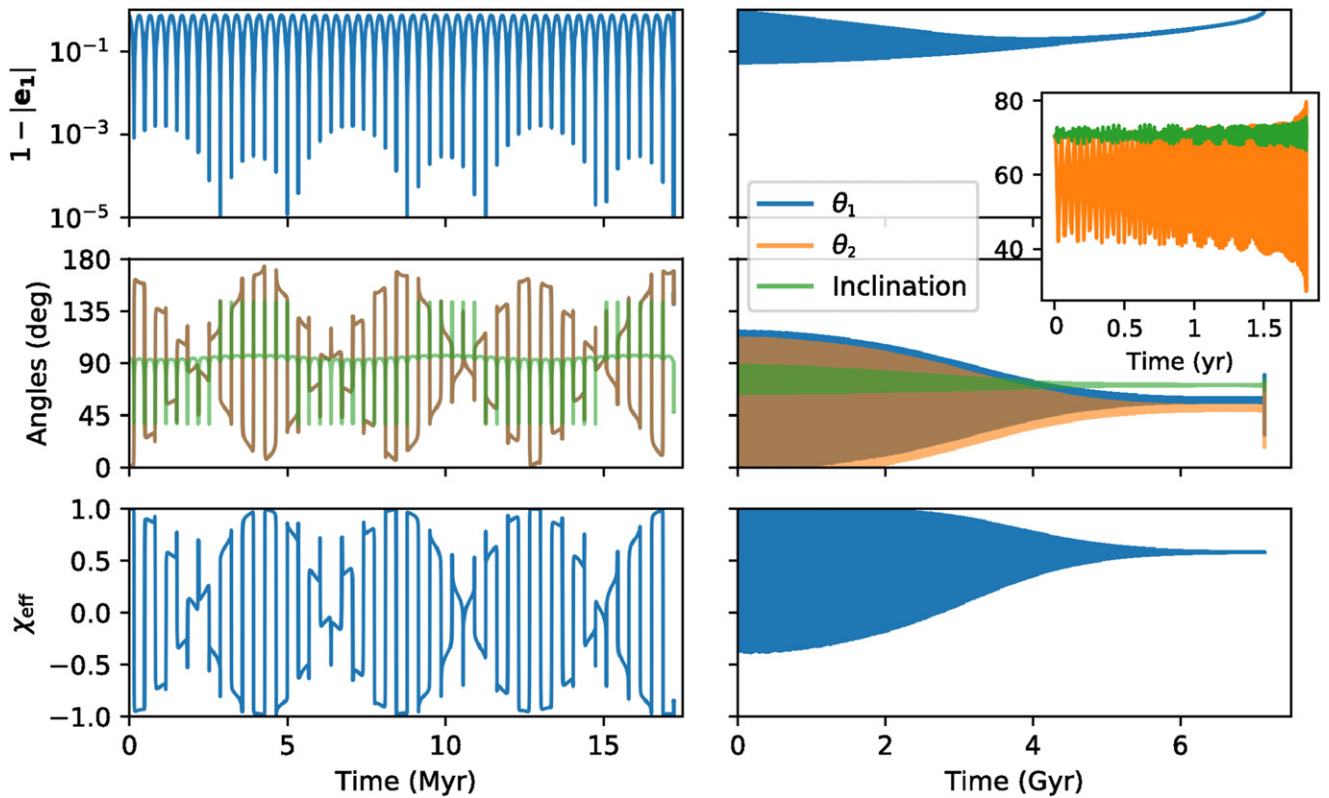
Figure 2. Two triple systems integrated to merger from our BH triple population described in Section 4. On the left, we show a triple where the eccentric LK mechanism pushes the inner binary to merge very rapidly (case (i) from Section 2.2). In this case, the spins remain essentially fixed in 3D space (with respect to the invariable plane) while the orbit of the inner binary oscillates wildly about them. On the right, we show an example where the spin precession and LK oscillations occur on a similar timescale. Here, the spin vectors smoothly precess onto the invariable plane of the triple (see Antonini et al. 2018), until both they and the inner binary are frozen at a given orientation due to the increased pericenter precession from the 1pN terms (case (ii)). Eventually this frozen binary merges due to GW emission. The inset shows the final changes in inclination and θ_2 arising from SO and SS effects, where the spins of the inner binary can couple to its orbital angular momentum (influencing the mutual inclination of the triple). These effects are not present in $\chi_{\rm eff}$, since the effective spin is a constant of the motion up to 2pN order.

barrier (Equation (29)) suppresses any trans-adiabatic behavior, and a_1 and e_1 slowly decrease over many LK cycles. In the right panels of Figure 2, we show an example of this type of evolution. Any highly eccentric oscillations and chaotic spin evolution are dampened by pericenter precession as the inner binary reaches high eccentricities. The spin vectors can precess onto the invariable plane of the triple (as described in Antonini et al. 2018), eventually freezing to a constant misalignment with respect to j_1 as the inner binary orbit decays due to GW emission to a region where pericenter precession completely suppresses LK oscillations, expression (28).

The condition for the transition between regimes (ii) and (i) can be derived by requiring $j_{\rm GR} < j_{\rm GW}$, which leads to

$$a_2 j_2 < \left(\frac{\pi c^2 a_1^4 m_3}{G(m_1 + m_2)^2} \right)^{2/5} \left(\frac{170}{3^7} \frac{G m_1 m_2 \nu^3}{c^5 a m_3} \right)^{1/15}. \qquad (32)$$

For systems that satisfy this condition, the 1pN terms are not important, since GW radiation will drive a fast inspiral of the BBH at $j \approx j_{\rm 2.5pN}$. Both of these cases have particular observable properties for Advanced LIGO/Virgo, which we will explore in Section 6.

3. Triple Population

Here we detail the initial conditions considered in this study, and describe our method for evolving massive stellar triples from their birth on the zero-age main sequence to the formation of BH triples. We start with a population of stellar triples with the following initial conditions: we draw the primary mass (m_1) of the inner binary from between $22\,M_\odot$ and $150\,M_\odot$ from a standard distribution given by $p(m)dm \propto m^{-\alpha}dm$, where $\alpha = 2.3$ (Kroupa 2001). The mass of the secondary (m_2) is assigned by assuming a uniform distribution of mass ratio, such that $m_2/m_1 = U(0, 1)$. The tertiary mass (m_3) is assigned in a similar fashion ($m_3/(m_1 + m_2) = U(0, 1)$). These samples are repeatedly drawn until the initial mass of each star lies between $22\,M_\odot$ and $150\,M_\odot$. The spins for all BHs are assumed to be maximal ($\chi = 1$) although we relax this assumption in Section 6.1.

The orbital properties for the inner and outer binaries are selected from two distinct populations: for the inner binaries, we use recent results on close binaries from Sana et al. (2012). The orbital periods for the inner binaries are drawn according to $(\log P)^{-0.55} d \log P$ where P is in days and $\log P$ is selected from 0.15 to 5.5. The eccentricity is drawn from a distribution given by $p(e)de \propto e^{-0.42}de$ from 0 to 0.9. For the outer binaries, we assign the semimajor axis from a distribution that is flat in $\log a$, while the eccentricity is drawn from a thermal distribution, $p(e)de \propto 2e\,de$. All the angles defining the triple (arguments of pericenter, longitudes of the ascending node, and the inclination) are drawn from isotropic distributions (with the longitude of the ascending node of the outer binary offset from the inner binary by π (i.e. $\Omega_2 = \Omega_1 - \pi$)).

To evolve our stellar triples to BH triples, we use a modified form of the binary stellar evolution (BSE) package from Hurley et al. (2002), including newer prescriptions for wind-driven

mass loss, compact object formation, and pulsational-pair instabilities (see details in Rodriguez et al. 2016a, 2018). Each triple is integrated by considering the inner binary and the tertiary as separate stellar systems. In other words, the binary is evolved using BSE, while the tertiary is evolved using the single stellar evolution (SSE) subset of BSE (Hurley et al. 2000). This, of course, does not account for the possibilities of mass accretion between the inner binary and the tertiary or any dynamical interaction between the inner and outer binaries (in other words, we do not consider any LK oscillations that the triples may experience before they become BH triples). Such physics, while interesting, is significantly beyond the scope of this paper (though again see Antonini et al. 2017 for a thorough analysis of such triples using the self-consistent method developed in Toonen et al. 2016). What we *are* interested in is the change to the orbital components due to the mass loss and BH natal kicks as the elements of the triple evolve toward their final BH states.

To compute this, we track the masses, radii, stellar types, BH natal kicks, and (for the inner binary) the semimajor axes and eccentricities as computed by BSE for every star/binary. Then, at every timestep, we expand the semimajor axis of the outer binary by an increment

$$\Delta a_2 = \left(\frac{\Delta M}{m_1 + m_2 + m_3} \right) a_2.$$

When a BH is formed, we extract the velocity of the natal kick as computed by BSE. The kick is then applied self-consistently to the orbital elements of the triple (see Appendix 1 of Hurley et al. 2002). Briefly, we assume that each natal kick occurs instantaneously (compared to the orbital timescale). When the kick occurs, we draw a random orbital phase from the mean anomaly. The kick is then applied instantaneously to the orbital velocity vector of that component. We compute the new angular momentum vectors (using the new orbital velocity vector and the same orbital position vector) and a new Laplace–Runge–Lenz vector, A. This gives us the new orientation of each binary in three-dimensional space, as well as the new semimajor axis and eccentricity, computed via

$$L_{new} = M_{new} r \times v_{new}$$
$$A_{new} = \frac{1}{GM_{new}} v_{new} \times L_{new} - \hat{r}$$

where M_{new} is the new mass of the binary after BH formation, and the new j and e vectors are simply L_{new}/L and A_{new}, respectively. The new semimajor axis is given by

$$a_{new} = \frac{2}{r} - \frac{v_{new}^2}{GM_{new}}.$$

If $a_{new} < 0$ or $e_{new} > 1$, the binary is disrupted.

Note that we must take care to apply the correct kick to each system. These kicks can be thought of as the combination of two effects: the actual change in velocity of one component arising from the asymmetric ejection of material, and the change in the orbital elements from the instantaneous loss of mass from a single component (Blaauw 1961). When the inner binary undergoes a supernova (SN), this mass loss can change the semimajor axis, eccentricity, and center-of-mass velocity of the binary. While most of the changes are naturally tracked by our above formalism, the change in the center-of-mass velocity of the inner binary must be explicitly recorded. This change is

then added to the velocity arising from the BH natal kick, and applied as V_{new} to the outer binary.

In addition to the masses and the evolution of the orbital elements, we implement several additional checks on the survival of our BH triples. We do not keep any triples that become dynamically unstable at any point during their integration, because a fully chaotic dynamical triple cannot be modeled by the secular evolution considered here (and would very likely result in a collision). We consider triples to be stable if they satisfy (Mardling & Aarseth 2001)

$$\frac{a_2}{a_1} > \frac{2.8}{1 - e_2} \left[\left(\frac{m_1 + m_2 + m_3}{m_1 + m_2} \right) \left(\frac{1 + e_2}{\sqrt{1 - e_2}} \right) \right]^{2/5}. \quad (33)$$

We also do not keep any triples that could potentially undergo a collision between their inner and outer components (BSE self-consistently tracks for collisions in the inner binary). For this, any triple where the pericenter distance of the outer binary can potentially touch the apocenter of the inner binary according to

$$a_2(1 - e_2) - R_3 < a_1(1 + e_1) + \max(R_1, R_2)$$

at any point during its evolution is discarded (where R_i are the radii of the stars).

Although we will discuss them in Section 4, we do not dynamically integrate any triple for which the LK mechanism will be strongly suppressed by the 1pN pericenter precession of the inner binary. For this, we simply exclude any triple for which Equation (28) is satisfied once all three objects have evolved to BHs. Finally, we explicitly exclude from our sample any triples whose inner binary would merge during a Hubble time due to GWs alone. This is done to limit ourselves to the population of "useful triples" (a term taken from Davies 2017), those that merge only due to the LK oscillations induced by the tertiary BH. Although there is likely a small population of merging BBHs whose dynamics may have been altered by a third companion, we do not consider them, in order to maintain a clean separation between the triple-driven BBH mergers studied here and the rate of mergers from common-envelope evolution in galactic fields.

4. Initial Population of BH Triples

4.1. Evolved BH Triples

We integrate a population of stellar triples using the formalism and initial conditions described in the previous section. We consider 11 different stellar metallicities ($1.5Z_\odot$, $Z_\odot$, $0.5Z_\odot$, $0.375Z_\odot$, $0.25Z_\odot$, $0.125Z_\odot$, $0.05Z_\odot$, $0.0375Z_\odot$, $0.025Z_\odot$, $0.0125Z_\odot$, and $0.005Z_\odot$), and integrate 10^5 different triples for each metallicity bin, for a total of 1.1×10^6 stellar triples.

Of immediate interest is the number of stellar triples that survive to become stable, hierarchical BH triples. Of our 1.1×10^6 triples, approximately 10% evolve from zero-age main-sequence triples to hierarchically stable (Equation (33)) BH triples without being disrupted due to mass loss or natal kicks, or undergoing stellar collisions. Of those, roughly half (5% of the initial population) form triples where the LK timescale is less than the precession timescale of the inner binary, and have the potential to undergo LK oscillations (Equation (28)). However, these results are highly dependent on the metallicity of the system.
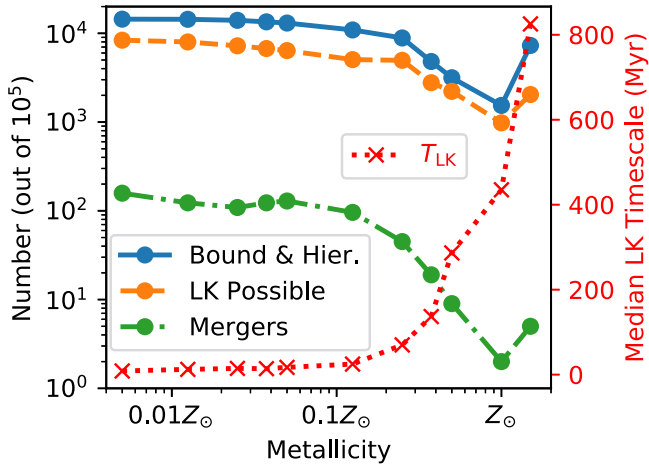
Figure 3. The efficiency of stellar triples at producing merging BBH triples as a function of metallicity. Each metallicity bin started with 10^5 stellar triples. Out of those, we show the number of triples for which the systems remain bound and hierarchical as they evolve from stars to BHs, the number of those BH triples for which LK oscillations are possible (according to Equation (28)), and the number of those BH triples which merge. We also show the median LK timescale (Equation (24)) in red for all of the LK-possible triples in each metallicity bin. The increase by a factor of ∼100 in the number of mergers at low metallicity arises from both the increased number of surviving BH triples and the decreased LK timescale of those triples.

In Figure 3, we show the number of systems in each metallicity bin that survive their evolution from stellar triple to BH triple to LK-induced merger (which we will explore in the next section). As the metallicity is increased, the number of systems that survive their evolution decreases dramatically, with nearly an order of magnitude fewer systems remaining as bound and hierarchical triples at solar metallicity than at lower (∼$0.01Z_\odot$) metallicities. This is entirely due to the mass loss and natal kicks experienced by massive stars at different stellar metallicities. Massive stars with high metallicities lose significant amounts of their mass during their evolution, largely due to radiation pressure in higher-opacity envelopes and line-driven winds (e.g., Vink et al. 2001). This mass loss expands the bound systems (such as binaries and triples), making each system more susceptible to disruption during stellar collapse. Furthermore, high-metallicity stars lose more mass, producing lower-mass cores and correspondingly lower-mass BHs. These systems are conjectured to experience large natal kicks during an SN, adding significant velocity kicks to the system (e.g., Fryer et al. 2012; Repetto & Nelemans 2015), while many of the massive BHs that form at lower metallicities are expected to form via direct collapse, experiencing little or no kick (Fryer & Kalogera 2001; Belczynski et al. 2016). The effect of metallicity is twofold: high-metallicity systems lose more mass during their evolution, significantly expanding their orbits, where the stronger natal kicks associated with these lower-mass BHs can more easily disrupt the outer orbits.

While the survival of BH triples increases by nearly a factor of 10 at low Z versus $Z_\odot$, the number of LK-induced mergers increases by almost a factor of 100. This additional increase is due to the decreased mass loss at lower metallicities, which reduces the expansion of both the inner and outer semimajor axes during the evolution of the triples. These tighter triples have significantly shorter LK timescales than triples at high metallicities. In Figure 3 (red axis) we show the median LK timescale (24) for the collection of bound and hierarchical
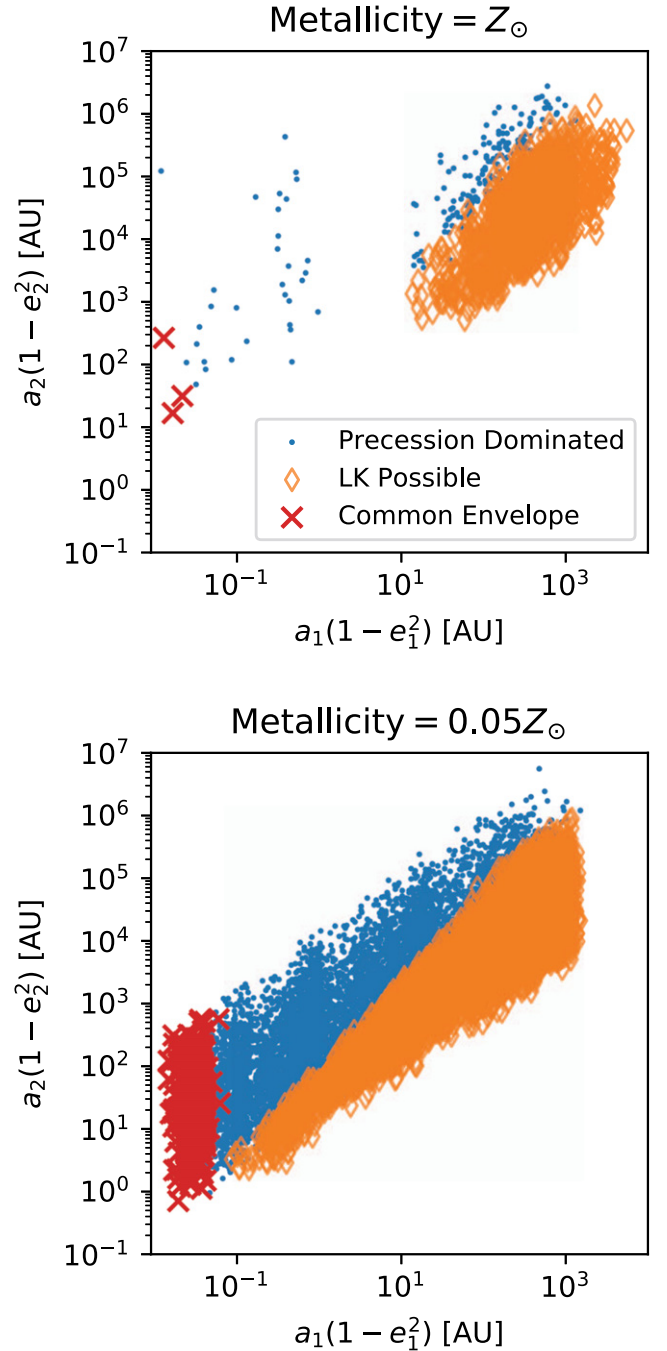

Figure 4. The final orbital parameters for the inner and outer binaries of all the bound BH triples at both solar and 5% solar metallicities. At solar metallicity, the increased mass loss from stellar winds drives both the inner and outer binaries to significantly larger separations (and correspondingly longer LK timescales) compared to low-metallicity systems. We separate the populations into triples that are precession-dominated, those for which LK oscillations are possible (Equation (28)), and those that have undergone a common-envelope phase of evolution. We find no post-common-envelope systems that have a sufficiently close tertiary companion to undergo LK oscillations.

triples in each metallicity bin. The typical LK timescale of the lowest metallicity triples is ∼100 times shorter than for those at solar metallicities. These triples will have many opportunities to experience highly eccentric oscillations (thousands per Hubble time) that may induce a merger, while high-metallicity systems may undergo only a few to tens of oscillations within the age of the universe.
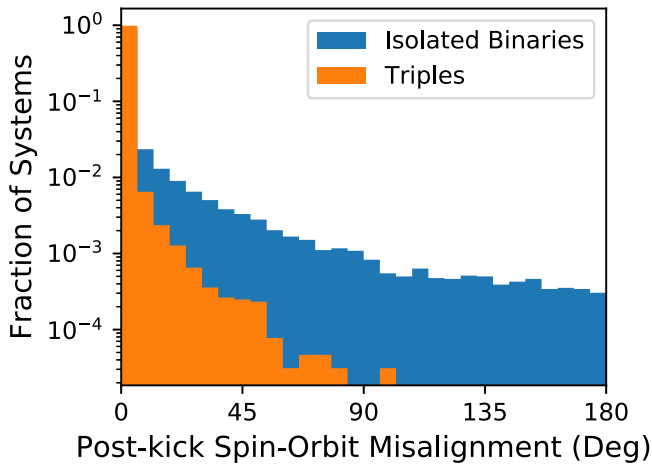
Figure 5. The misalignments between the spins of the two BHs and the angular momentum of the inner binary (θ_1 and θ_2) after the triple has evolved to a stable BH triple, assuming the initial stellar spins were aligned with j_1. We show the final misalignments for all the inner binaries that were evolved (regardless of whether the tertiary remained bound and hierarchical), and for all the triples. The triple population has a significant preference for spin alignment, since any natal kick capable of significantly torquing j_1 would also likely disrupt the weakly bound tertiary companion.

Figure 6. The distribution of effective spins for merging BBHs. We show the distribution for triples with varying levels of spin physics. We consider triples with no spin effects, only 1pN precession of the spins (Equation (17)), all SO terms (Equations (15)–(17)), and all SO and SS terms (Equations (15)–(20)). Considering only the 1pN "de Sitter" precession of the spins is clearly sufficient for most cases, since the higher-order SO and SS terms to not play a significant role until immediately before merger. The filled gray histogram shows χ_{eff} if the spins were completely isotropic (but using the mass distribution from our population synthesis).

In Figure 4, we show the orbital parameters of the inner and outer binaries for those bound and hierarchical triples in our $Z_\odot$ and $0.05Z_\odot$ models. While the minimum value of $a_1(1 - e_1^2)$ at solar metallicity for LK-driven mergers is ~ 10 au, the low-metallicity triples span the allowed range of inner orbits from 0.1 to $10^3 a_1(1 - e_1^2)$. Below 0.1, we find that all BH triples are suppressed from undergoing LK oscillations by the pericenter precession of the inner binary. We note that this includes all systems for which the inner binary has undergone a common-envelope phase of evolution. Although we find many post-common-envelope systems in our 1.1×10^6 triples, they all inhabit the region of parameter space (Equation (28)) where pericenter precession quenches any possibility of LK oscillations.

4.2. Initial BH Spin-misalignment

Although the formalism presented in Section 2 allows us to track the evolution of the spin vectors for the hierarchical three-body problem, the initial amount of misalignment between the BH spins and the angular momentum of the inner binary must be treated carefully. While we assume that the initial stellar spins are aligned with j_1, it is well known that the BH kicks can significantly misalign the orbital and spin angular momenta (e.g. Kalogera 2000), since any instantaneous kick to one of the binary components will change the direction of the orbital angular momentum. Fortunately, the formalism presented in Hurley et al. (2002) and employed here makes it trivial to track the change in orientation of j_1 through the two SNe of the inner binary (the outer binary kick cannot torque the inner binary).

In Figure 5, we show the post-kick misalignments of the BH spins with j_1, assuming that SN kicks are emitted isotropically in direction from the surface of the exploding stars, and that neither mass transfer nor tidal torques can realign either the stellar or BH spin with the orbit after the natal kick. These are both highly conservative assumptions that allow us to explore the maximum allowed post-SN misalignment (see Rodriguez et al. 2016c). We find that the vast majority of post-kick misalignmen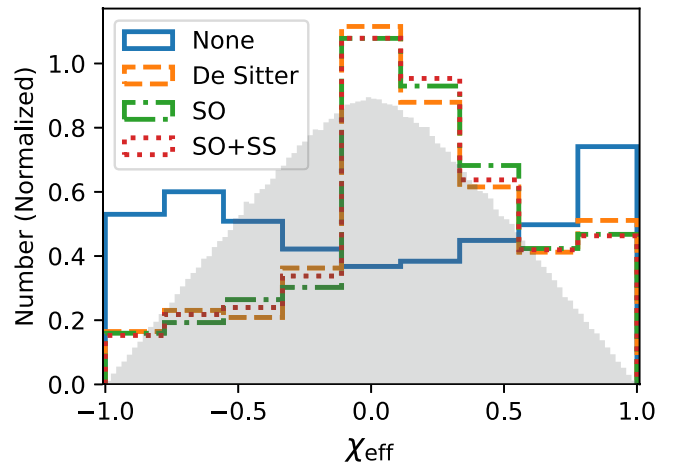ts are very small, with 97% of systems having misalignments less than $0°.1$, and 99% of systems having misalignments less than $6°$. On the other hand, the misalignments of the isolated binaries themselves (ignoring whether the third BH remains bound) can be significantly larger, with $\sim 8\%$ of binaries having misalignments greater than $6°$ (in agreement with Rodriguez et al. 2016c). This increased preference for aligned triples arises from the difficulty of keeping the outer companion bound to the inner binary after the SN. While the semimajor axes for the inner binaries are sufficiently small for the binary to survive the kick, the outer orbits are so wide that the SN kicks are frequently several times larger than the typical orbital velocities for the outer orbits (usually a few km s^{-1}). Since smaller kicks produce smaller spin–orbit misalignments, the requirement that the tertiary companion remains bound significantly limits the possible range of initial misalignments.

Because of that, and the associated difficulties of following spin realignment through mass transfer and tidal torques, we will assume that our BH triple systems begin with their BH spins aligned with j_1 (although we test the implications of this assumption in Figure 7).

5. Spin Distributions of Useful Triples

We now turn to understanding the spin distributions of merging triple systems formed from stellar triples. As stated previously, we are interested in the distribution of "useful" triples, which we define to be those mergers whose inner binaries would not have merged in a Hubble time as an isolated system. We focus mainly on the distributions of χ_{eff} (Equation (21)), because this is the spin parameter most easily measured by Advanced LIGO/Virgo. The first question that naturally arises is whether the inclusion of higher-order pN corrections (the SO and SS terms) has a significant influence on the final measurable values of χ_{eff}. It was claimed in Liu & Lai (2017, 2018) and Antonini et al. (2017) that the lowest-order precession of the spin vectors about j_1 (also known as geodetic or de Sitter precession) would dominate the spin dynamics of the system, and the higher-order terms (such as the Lense–
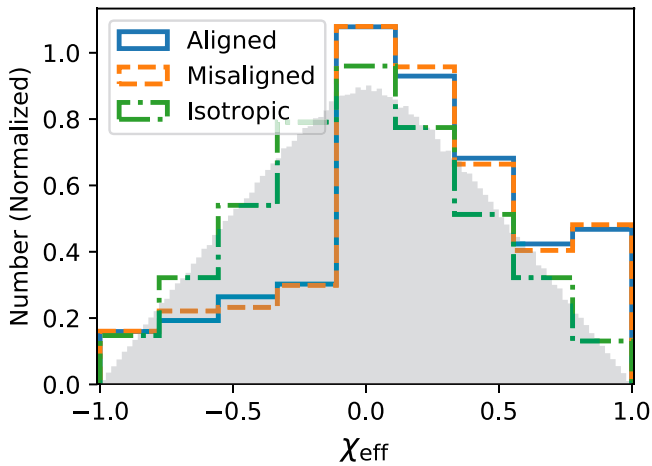
Figure 7. Similar to Figure 6 (with all spin terms), but considering different initial spin alignments for the inner BBHs. We show the final $\chi_{\rm eff}$ distributions for BBHs that are perfectly aligned with j_1, those that begin with some misalignment based on BH natal kicks (Figure 5), and a completely isotropic initial distribution. The aligned and misaligned distributions are virtually identical, largely because the initial misalignments are extremely small. The initially isotropic distribution yields a final distribution that is also isotropic.

Figure 8. Joint total mass $(m_1 + m_2)$ and effective spin distributions for merging BBHs. We also show each of the measured posteriors for $M_{\rm tot}$ and $\chi_{\rm eff}$ for each of the five BBH mergers (and one BBH merger candidate) reported by LIGO/Virgo so far.

Thirring/SO coupling or the SS coupling) would not significantly affect the dynamical evolution.

In Figure 6, we show the $\chi_{\rm eff}$ distributions of our useful triples, and how they vary depending on the sophistication of the SO physics considered. As expected (Antonini et al. 2017), there is a significant difference between the triples integrated with no spin terms and those integrated by considering de Sitter precession (which we simulate by including all SO terms, but setting $\chi_1 = \chi_2 = 0$, allowing the spin vectors to precess but not couple to the orbits).

Figure 6 also makes clear that the inclusion of the full SO and SS terms does not play a significant role in the final distribution of the measurable spin terms. This is fully consistent with the discussion in Section 2.2: any triple for which the separation during LK oscillations would get small enough for SO or SS effects to become relevant will immediately decouple from the tertiary and merge due to the GW emission. This "case (i)" type of merger is illustrated in the left panel of Figure 2. On the other hand, for any case where the LK oscillations remain relevant during the inspiral, the 1pN pericenter precession will suppress any higher-order pN effects until the binary effectively decouples from the third companion ("case (ii)", or the right panels of Figure 2). In other words, there exists no regime in which the SO or SS terms are relevant for the distributions of $\chi_{\rm eff}$.

We have also assumed that the initial spin distributions of the BHs are aligned with j_1 at the beginning of the LK evolution of the triple. We showed in Section 4.2 that, due to the natal kicks, the vast majority of bound and hierarchical BH triples have spins initially aligned with j_1 (assuming the spins of the stars were initially aligned with j_1). In Figure 7, we show $\chi_{\rm eff}$ for the same population integrated with all spin terms, but with different initial orientations for the spins. As expected, the initial misalignments for the stellar triples make little difference in the final $\chi_{\rm eff}$ distributions. However, we also find that, if the distribution of initial spins is isotropic (as would be expected for dynamically assembled triples, e.g., Antonini & Rasio 2016), then the final distribution of spins is also isotropic. This is to be expected, since it is well known that an isotropic
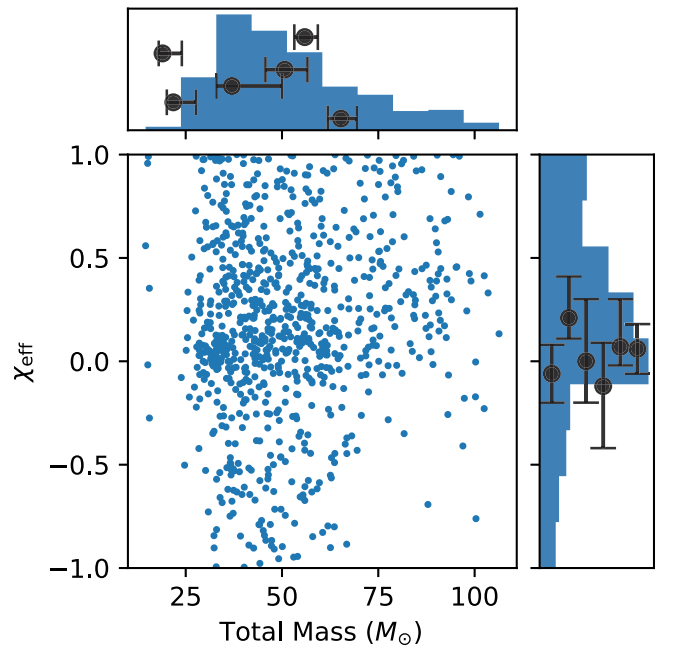
distribution of spins will remain isotropic during inspirals of isolated binaries (Schnittman 2004), and there is no reason to expect differential precession of the two spin vectors by de Sitter precession (which dominates the spin evolution during LK oscillations) to create a preferred direction from an isotropic distribution.

6. Gravitational-wave Observables

6.1. Masses and Spins

The first obvious observable parameters that can be explored by the current generation of gravitational-wave detectors are the masses and the spins of the merging BHs. As mentioned previously, the spin parameter most easily measured by Advanced LIGO/Virgo is the effective spin parameter, $\chi_{\rm eff}$. One can immediately ask whether there is any immediate correlation between the masses and the effective spins of our merging triples.

In Figure 8, we show the 2D distributions of the total mass versus the effective spin. There is no strong correlation between the effective spin and the total mass for the population of triple-driven mergers surveyed here. This is to be expected, since the LK timescale (24) is much more strongly dependent on the angular momentum of the outer binary than on the masses of the triple components. While this may not hold for more massive systems (such as a stellar-mass BBH in orbit around a supermassive BH), there is no significant correlation for the cases considered here. We do note that this model naturally explains all of the heavy BBHs observed to date (those with total masses $\gtrsim 40\,M_\odot$) along with their correspondingly low effective spins.

Throughout this analysis, we have assumed that the spins of the BBHs are maximal. This was done for simplicity, but we can also consider the effect of spin magnitudes on our predictions for $\chi_{\rm eff}$. Because we have shown that the SO and
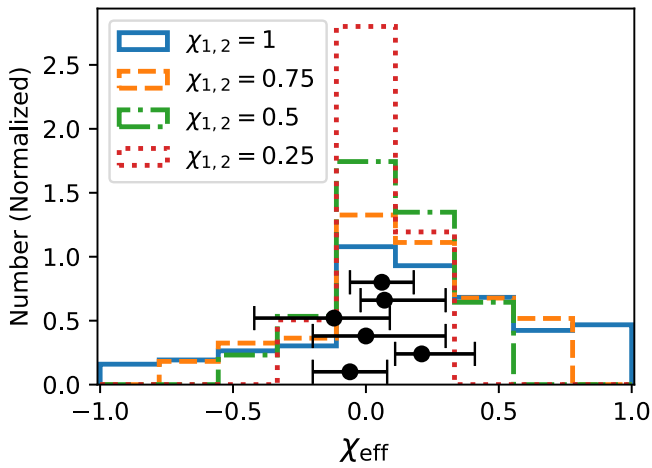
Figure 9. The same as the top panel of Figure 8, but now showing the $\chi_{\rm eff}$ distribution as a function of different spin magnitudes, calculated using the same final spin angles as in the previous section. Although this ignores the reduced SO coupling from the lower spin magnitudes, we have shown (Figure 6) that the SO and SS couplings do not influence the distributions of $\chi_{\rm eff}$, and the 1pN precession of the spins is independent of the spin magnitudes. The black points and their error bars show the six $\chi_{\rm eff}$ measurements reported by LIGO/Virgo so far.

Figure 10. Final distributions of the individual spin vectors with respect to j_1. We show the absolute misalignment between S_1 and j_1, θ_1, the relative misalignment angles between S_1 and S_2 along the azimuth, ($|\theta_1 - \theta_2|$), and the angle between the two spins in the orbital plane of the binary (perpendicular to j_1), $\Delta\phi$.

SS terms have a negligible effect on the spin evolution (while the precession of the spins about j_1 is independent of the spin magnitudes), for $\chi_{\rm eff}$ in these systems we can to a good approximation simply replace the spin magnitudes in our integrated $\chi_{\rm eff}$ distributions, to determine what $\chi_{\rm eff}$ would have been with lower spins. We show these values in Figure 9. As the spin magnitudes are decreased, the distribution of $\chi_{\rm eff}$ converges to zero, as would be expected for systems with low spins lying in the plane.

While we have focused on the effective spin of the BBHs, in reality the spin information is much more complex. It has been suggested (Gerosa et al. 2013, 2014; Trifirò et al. 2016) that a complete measurement of the BBH spin angles will allow Advanced LIGO/Virgo not only to discriminate between different formation channels for BBHs, but also to measure differences in the binary stellar physics producing BBH mergers from isolated field binaries.

In Figure 10, we show the distributions of θ_1, $|\theta_1 - \theta_2|$, and $\Delta\phi$. Both θ_1 and $\Delta\phi$ have broad distributions. The former arises from spin precession described in the previous sections, while the latter is a natural feature of randomly distributed vectors in the plane (see, e.g., Gerosa et al. 2013, their Figure 2). At the same time, we note that our distribution of $|\theta_1 - \theta_2|$ is somewhat broader than the one presented there. This suggests that sufficient observations of the individual spin angles can be used not only to better understand BSE, but also to discriminate between binary and triple stellar evolution of BBH mergers (e.g., Trifirò et al. 2016).

6.2. Eccentricity and Spin

The eccentricity distribution of BBHs from LK-induced mergers is one of the distinct observables that can be identified by GW detectors. While BBHs from isolated field binaries and BBHs ejected from globular clusters will reach the LIGO/Virgo band with very low orbital eccentricities ($\lesssim 10^{-3}$, e.g., Breivik et al. 2016), the presence of the third companion can induce highly eccentric mergers that can maintain eccentricities as high as $e \sim 0.1$ up to a GW frequency of 10 Hz (assuming
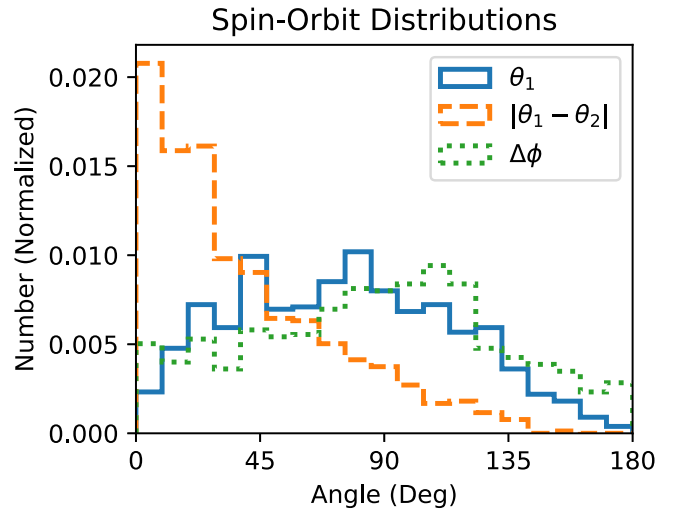
the secular approximation to be valid, e.g., Antonini et al. 2014). How these values correlate with the spins can be a significant discriminant between BBH formation channels.

In Figure 11, we show the 1D distributions for the eccentricity at a GW frequency of 10 Hz (the lower bound of the LIGO band) and their corresponding $\chi_{\rm eff}$ distributions. There is a clear break at $e_{\rm 10Hz} \sim 2 \times 10^{-4}$, where binaries with higher eccentricities have a nearly flat distribution in $\chi_{\rm eff}$ from -1 to 1, while binaries with lower eccentricities recover the $\chi_{\rm eff} \sim 0$ peak described in the previous sections. This behavior is discussed at length in Section 2.2, and is well illustrated in Figure 2. In the example of case (i) (left panels), the strong octupole terms from the interaction Hamiltonian drive the eccentricities to very large values ($e_1 > 0.99999$) such that GW emission drives the binary to merge before the 1pN terms can significantly dampen the LK oscillations or cause the spins to precess. At the same time, the inner binary can flip its angular momentum several times, while the spin–orbit angles vary wildly. When this binary merges (essentially in a single highly eccentric oscillation), the spins are still aligned with each other, while the spin–orbit orientation is drawn from a nearly random distribution from 0 to 180°. This type of evolution results in the uniform $\chi_{\rm eff}$ distribution of the higher eccentricity systems displayed in Figure 11. On the other hand, the smoother evolution of case (ii) in the right panels of Figure 2 does not experience large oscillations in eccentricity/inclination, since any highly eccentric oscillations are arrested by the angular momentum barrier (Equation (32)). This significantly longer evolution allows the spins to experience significant precession, producing a $\chi_{\rm eff}$ near 0.5 (Antonini et al. 2018), while the angular momentum barrier keeps the maximum eccentricity at lower values, yielding a lower eccentricity at merger. We show the fraction of systems that obey Equation (32) as a function of eccentricity in the top panel of Figure 11.

We do note that, by restricting ourselves to the secular equations of motion, we have explicitly ignored the highly eccentric mergers that can occur during LK oscillations when the secular approximation breaks down (e.g., Antonini et al. 2014).
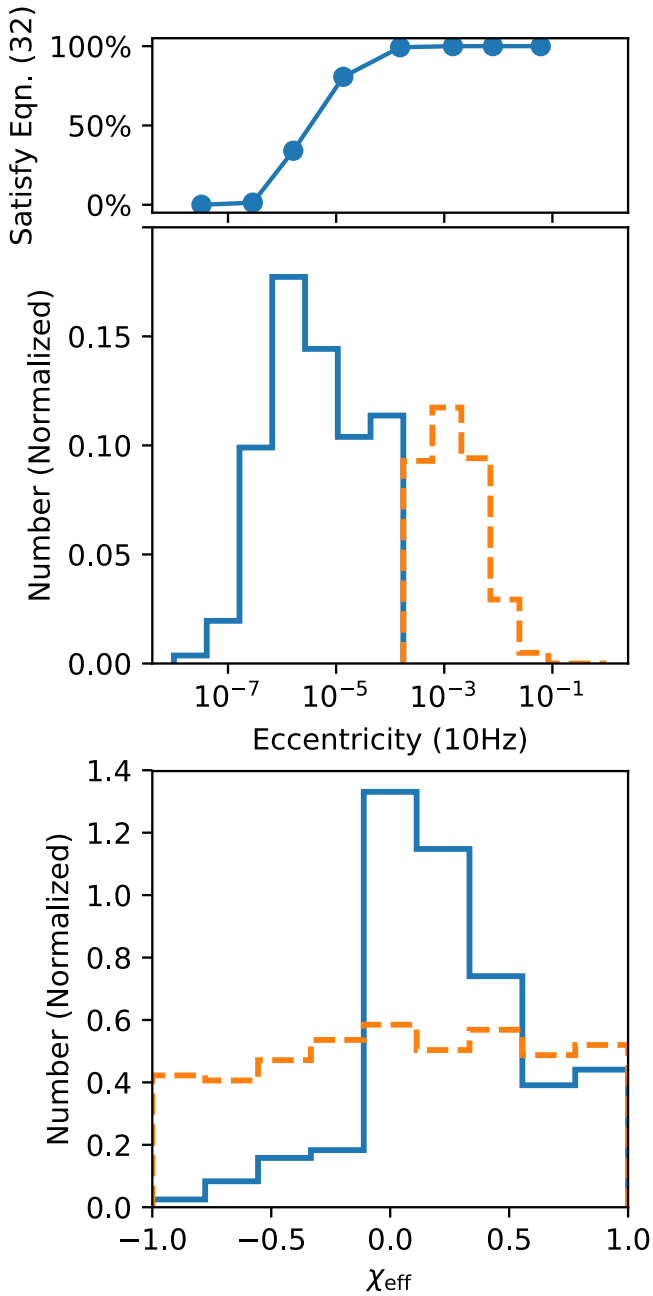
Figure 11. The final eccentricity (at a GW frequency of 10 Hz) and $\chi_{\rm eff}$ distributions from merging BBHs. On the top, we show the eccentricity distributions above and below 2×10^{-4} (in solid blue and dashed orange), while the inset along the top shows what fraction of the triples at each eccentricity initially satisfies Equation (32). On the bottom, we show the $\chi_{\rm eff}$ distributions corresponding to those same eccentricity bins. For high-eccentricity systems, the distribution is nearly flat, while low-eccentricity distributions clearly show the distinct $\chi_{\rm eff}$ distribution shown in the text. An example from each of these distributions is shown in Figure 2, in the left and right panels respectively.

Since the breakdown occurs in regimes where very high eccentricities allow GW emission to change the triple on an orbital timescale, these systems (with $e_{10\rm Hz} \sim 1$) would likely show a similarly flat distribution in $\chi_{\rm eff}$.

6.3. Merger Rate

To probe the contribution from this channel to the population of BBH binaries detected by Advanced LIGO/Virgo, we place
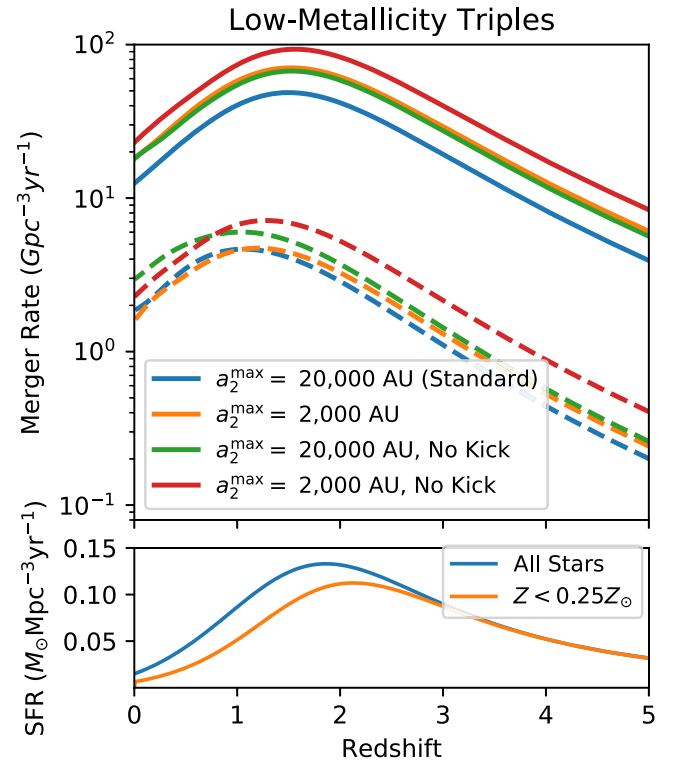

Figure 12. The merger rate of low-metallicity BH triples as a function of cosmological redshift. In the top panel, we show the four variant triple BH populations described in the main text (Section 6.3). We bracket the uncertainties in our triple stellar evolution by assuming that (i) no triples merge or interact during their main-sequence evolution (solid lines), or (ii) any stellar triple that can undergo LK oscillations with an LK timescale <3 Myr merges during its main-sequence evolution (dashed lines) and is excluded from our rate estimate. The pessimistic criterion preferentially selects triples with longer delay times between formation and merger, which in turn pushes the peak of the pessimistic estimate to lower redshifts. In the bottom panel, we show our assumed SFR, and the SFR rate when restricted to metallicities below $0.25Z_\odot$ (Equations (34)–(36)).
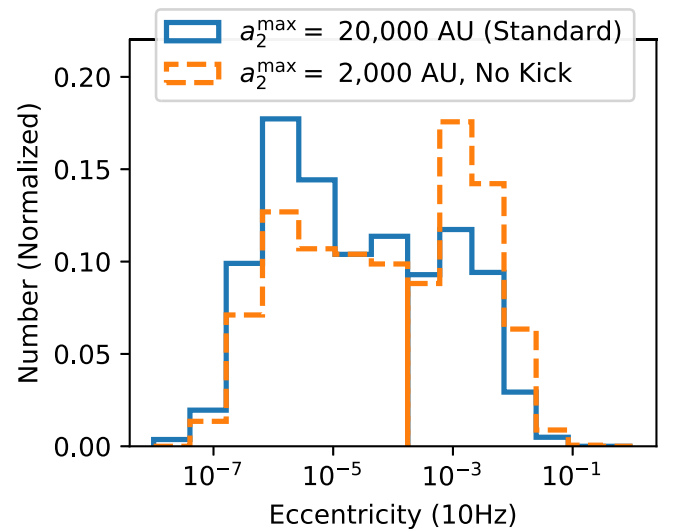

Figure 13. The final eccentricity (at a GW frequency of 10 Hz) for our standard model (used throughout the main text) and our more liberal model (maximum a_2 of 2000 au and no BH natal kicks). While the underlying physics of these two distributions is unchanged (see Sections 2.2 and 6.2), the relative number of systems in each peak (determined by Equation (32)) depends on our initial conditions.

our models of BH triples into a cosmological context. We begin by assuming that the formation of stellar BH triples will follow the cosmological SFR of the universe. We use the SFR as a function of redshift from Belczynski et al. (2016), based on significant multi-wavelength observations (see, e.g., Madau & Dickinson 2014):

$$\mathrm{SFR}(z) = 0.015 \frac{(1+z)^{2.7}}{1 + ((1+z)/2.9)^{5.6}} \, M_\odot \, \mathrm{Mpc}^{-3} \, \mathrm{yr}^{-1}. \quad (34)$$

Because we have shown that the contribution from low-metallicity star formation is the dominant contribution to the BH triple channel (e.g., Figure 3), we consider only the SFR for stars with $Z < 0.25 Z_\odot$. This is done by computing the cumulative fraction of star formation, using the chemical enrichment model of Belczynski et al. (2016). In this model, the mean metallicity Z at a given redshift z is given by

$$\log_{10} \langle Z(z) \rangle = 0.5 + \log_{10} \left[\frac{y(1-R)}{\rho_b} \right.$$
$$\left. \times \int_z^{20} \frac{97.8 \times 10^{10} \mathrm{SFR}(z')}{H_0 E(z')(1+z')} dz \right] \quad (35)$$

where $R = 0.27$ is the fraction of mass from each generation of stars that is returned to the interstellar medium, $y = 0.019$ is the mass fraction of new metals created in each generation of stars, $\rho = 2.77 \times 10^{11} \Omega_b h_0^2 \, M_\odot \, \mathrm{Mpc}^{-3}$ is the baryon density with $\Omega_b = 0.045$ and $h_0 \equiv H_0/100$, and $E(z) \equiv \sqrt{\Omega_M (1+z)^3 + \Omega_k (1+z)^2 + \Omega_\Lambda}$.

Belczynski et al. (2016) assumed that the distribution of metallicity at a given redshift followed a log-normal distribution, with mean given by (35) and a standard deviation of 0.5 dex (based on measurements from Dvorkin et al. 2015). Since we are only interested in metallicity below $0.25 Z_\odot$, and since we are dealing with small number statistics, we convolve the SFR from (34) with the cumulative distribution of metallicities:

$$\mathrm{SFR}_{Z < Z_{\mathrm{low}}}(z) = \mathrm{SFR}(z)$$
$$\times \left(1 + \mathrm{erf} \left[\frac{\log_{10}(Z_{\mathrm{low}}) - \log_{10} \langle Z(z) \rangle}{0.5\sqrt{2}} \right] \right). \quad (36)$$

For this estimate, we restrict ourselves to models for which $Z < 0.25 Z_\odot$ (see the bottom panel of Figure 12). We then assume that the rate can be expressed as

$$R(z) = F_{\mathrm{merge}} F_{\mathrm{triple}} F_{M > 22 M_\odot} \langle M_\star \rangle$$
$$\times \int_{-\infty}^{\infty} t_{\mathrm{delay}}(t(z) - t') \mathrm{SFR}_{Z < Z_{\mathrm{low}}}(z(t')) dt' \quad (37)$$

where F_{merge} is the fraction of triples that merge (e.g., Figure 3), F_{triple} is the fraction of massive binaries with a tertiary companion (taken to be 60%, following Sana et al. (2014), their Figure 16), $F_{M > 22 M_\odot}$ is the fraction of triples with all three components having masses above $22 M_\odot$ (assuming m_1 is drawn from the initial mass function, while m_2 and m_3 are drawn from distributions uniform in the mass ratio), $\langle M_\star \rangle$ is the mean mass of a star from the initial mass function (both taken from Kroupa (2001), running from $0.01 M_\odot$ to $150 M_\odot$), and t_{delay} is the distribution of delay times between triple formation and merger. The integral is the convolution of the distribution of delay times over the low-metallicity SFR. The factors $z(t)$

and $t(z)$, giving the redshift at a given lookback time and vice versa, ensure that the integral is performed over time, and that the corresponding rate is in mergers per unit time (not per unit redshift).

Here we introduce three new sets of initial conditions, designed to bookend the possible parameter space of rates. In addition to our standard model, in which the distribution of outer orbits runs up to 20,000 au, we also consider a population synthesis model with a maximum initial a_2 of 2000 au. Furthermore, because the kicks are one of the largest uncertainties in many population synthesis studies of BBHs, we also consider models with zero natal kicks for any BHs (though we still treat the effect of the mass loss of the inner binary). The four possible models are presented in Figure 12.

The second critical uncertainty is the possible LK dynamics during the evolution of the stellar triples to BH triples, which we have ignored here. To bracket this uncertainty, we consider two additional factors: first, for the most pessimistic case, we assume that any stellar triple whose initial LK timescale is less than the lifetime for the most massive stars (~ 3 Myr) will merge before it evolves to a BH triple. We then exclude from our sample any triple where $t_{\mathrm{LK}} < 3$ Myr and Equation (28) is false, since a stellar triple may begin its life sufficiently close that pericenter precession suppresses LK oscillations (and possible mergers), then evolve to a regime where LK is possible. This assumption reduces the overall number of mergers by 90% to 95%, but is far more drastic than the results from the triple stellar evolution presented in Antonini et al. (2017), which found the decrease in surviving BH triples to be around 70% (see, e.g., their Figure 2). For the pessimistic case, we recompute the rate using t_{delay} of those triples that cannot merge as stellar triples.

As is obvious from the figure, the rate increases with the overall SFR of the universe, peaking at around $z \sim 1.6$ for the optimistic cases and $z \sim 1.2$ for the pessimistic cases. The delay between the merger rate and the overall peak of low-metallicity SFR (at $z \sim 2$) arises from the delay time between formation of stellar triples and the merger of the inner BBH. The pessimistic case has a peak at lower redshifts, since we have assumed that triples with small LK timescales will merge during the main sequence, which leaves us with a population of mergers with longer delay times. The highest merger rate in any of our models (maximum a_2 of 2000 au and no BH natal kicks) occurs at $z \sim 1.6$, and is nearly 90 Gpc^{-3} yr^{-1}, which decreases to 23 Gpc^{-3} yr^{-1} in the local universe ($z \sim 0$). Our most pessimistic case (maximum a_2 of 2000 au, regular natal kicks, and excluding any systems where $t_{\mathrm{LK}} < 3$ Myr) achieves a maximum of 5 Gpc^{-3} yr^{-1} at $z \sim 1.1$, which decreases to 2 Gpc^{-3} yr^{-1} in the local universe. Combined with the rate of mergers from triples at solar metallicities (0.3–2.5 Gpc^{-3} yr^{-1} in the local universe, Antonini et al. 2017), this suggests an overall merger rate from stellar triples of between 2 and 25 Gpc^{-3} yr^{-1}. Although we do not show the calculation here, our high-metallicity stellar triples ($Z > 0.25 Z_\odot$) produce a similar merger rate of 0.1–2 Gpc^{-3} yr^{-1}.

This range of merger rates is consistent with the current rates from the first observing run of Advanced LIGO (Abbott et al. 2016a), but we note that this merger rate applies *only* to the heavy, low-spin BBH mergers detected to date. Given that these rates are fully consistent with the rate reported by these individual events (2–53 Gpc^{-3} yr^{-1} for GW150914-type events), we suggest that the merger of stellar triples from

low-metallicity environments can naturally explain all the heavy BBHs observed by LIGO/Virgo.

Finally, we note that these different initial conditions all show similar distributions of spin, mass, and eccentricity to those of our standard model that were illustrated in the previous section, with one notable exception. In Figure 11, the correlation between the eccentricity and spin of the system was set by the initial LK and GR timescales for each triple (Equation (32)). While the physics does not change with different initial conditions, the initial timescales do, which can alter the distributions of eccentricity and spin. We illustrate this in Figure 13, where we show the eccentricity distributions at 10 Hz for our standard model (i.e., the middle panel of Figure 13) and our most liberal model (maximum a_2 of 2000 au and no BH natal kicks). While the locations of the two peaks are unchanged (as are their respective χ_{eff} distributions), the relative fraction of sources in each regime of Equation (32) does change. As such, our somewhat conservative choice of initial conditions used in Section 6 may be underpredicting the number of sources with large eccentricities and a flat distribution of χ_{eff}.

7. Conclusion

In this paper, we have explored the contribution to the GW landscape from BBHs driven to merger by a third BH via the LK mechanism. By evolving a population of $\sim 10^6$ stellar triples, we found that the reduced mass loss and lower natal kicks for triples at low metallicities ($\lesssim 0.25 Z_\odot$) make stellar-mass BH triples nearly 100 times more efficient at producing mergers than triples at solar metallicities (e.g., Antonini et al. 2017). Using self-consistent secular equations for the triple dynamics and BBH spin evolution, we expand upon the results first described in Antonini et al. (2018), and show that these low-metallicity-forged triples naturally form heavy BBHs with low effective spins that merge in the local universe, and that the merger rate of these objects ($2-25\,\mathrm{Gpc}^{-3}\,\mathrm{yr}^{-1}$) can explain all of the heavy BBH mergers observed by LIGO/Virgo to date.

Our simplified approach to triple dynamics ignores the potentially significant evolution of stellar triples during their evolution to BH triples. Although our rate estimate brackets the range of possible mergers and interactions during this phase, a more self-consistent approach (e.g., Toonen et al. 2016) will provide further insight into the initial conditions of these systems, since it is likely that our upper limits have underestimated the number of stellar triples that merged before becoming triple BHs.

At the same time, we have ignored a significant amount of the LK-driven BBH merger parameter space by our assumption that the third body be a BH. This was done for simplicity (as our technique could not follow LK oscillations while a tertiary was still evolving), but the eccentric LK mechanism does not require the third body to be a BH. It is entirely possible that, by considering triples in which the inner BH binary is orbited by a distant massive star, the merger rates quoted here may increase.

Finally, all of our χ_{eff} distributions rely on the assumption that the spins of the inner binary are initially aligned with the orbit. Although this assumption has been used in many previous studies, it is easy to imagine scenarios where this may not be the case, and there exists some observational evidence that "Binaries are Not Always Neatly Aligned" (the BANANA survey, Albrecht et al. 2011, 2013, 2014). At the same time, many of the inner binaries in the triples explored here experienced significant mass transfer during their main-sequence evolution, which could, in conjunction with tidal torques, both spin-up and align the BHs with the orbital angular momentum. The correct treatment of dynamical tides and eccentric mass transfer during LK oscillations is significantly beyond the scope of this paper, but could play a large role in the initial spin distributions of BH triples.

ORCID iDs

Carl L. Rodriguez ⓘ https://orcid.org/0000-0003-4175-8881
Fabio Antonini ⓘ https://orcid.org/0000-0003-3138-6199

References

Abbott, B. P., Abbott, R., Abbott, T. D., et al. 2016a, PhRvX, 6, 041015
Abbott, B. P., Abbott, R., Abbott, T. D., et al. 2016b, PhRvL, 116, 241103
Abbott, B. P., Abbott, R., Abbott, T. D., et al. 2016c, PhRvL, 116, 061102
Abbott, B. P., Abbott, R., Abbott, T. D., et al. 2017a, PhRvL, 118, 221101
Abbott, B. P., Abbott, R., Abbott, T. D., et al. 2017b, ApJL, 851, L35
Abbott, B. P., Abbott, R., Abbott, T. D., et al. 2017c, PhRvL, 119, 161101
Ade, P. A. R., Aghanim, N., Arnaud, M., et al. 2016, A&A, 594, A13
Ajith, P., Hannam, M., Husa, S., et al. 2011, PhRvL, 106, 241101
Albrecht, S., Setiawan, J., Torres, G., Fabrycky, D. C., & Winn, J. N. 2013, ApJ, 767, 32
Albrecht, S., Winn, J., Carter, J., Snellen, I., & de Mooij, E. 2011, ApJ, 726, 68
Albrecht, S., Winn, J. N., Torres, G., et al. 2014, ApJ, 785, 83
Antonini, F., Murray, N., & Mikkola, S. 2014, ApJ, 781, 45
Antonini, F., & Perets, H. B. 2012, ApJ, 757, 27
Antonini, F., & Rasio, F. A. 2016, ApJ, 231, 187
Antonini, F., Rodriguez, C. L., Petrovich, C., & Fischer, C. L. 2018, MNRAS, 480, L58
Antonini, F., Toonen, S., & Hamers, A. S. 2017, ApJ, 841, 77
Askar, A., Szkudlarek, M., Gondek-Rosińska, D., Giersz, M., & Bulik, T. 2016, MNRAS, 464, L36
Bae, Y.-B., Kim, C., & Lee, H. M. 2014, MNRAS, 440, 2714
Banerjee, S. 2017, MNRAS, 467, 524
Banerjee, S., Baumgardt, H., & Kroupa, P. 2010, MNRAS, 402, 371
Barker, B. M., & O'Connell, R. F. 1975, PhRvD, 12, 329
Bartos, I., Kocsis, B., Haiman, Z., & Márka, S. 2017, ApJ, 835, 165
Belczynski, K., Dominik, M., Bulik, T., et al. 2010, ApJL, 715, L138
Belczynski, K., Holz, D. E., Bulik, T., & O'Shaughnessy, R. 2016, Natur, 534, 512
Belczynski, K., Kalogera, V., & Bulik, T. 2002, ApJ, 572, 407
Blaauw, A. 1961, BAN, 15, 265
Blaes, O., Lee, M. H., & Socrates, A. 2002, ApJ, 578, 775
Breivik, K., Rodriguez, C. L., Larson, S. L., et al. 2016, ApJL, 830, L18
Buonanno, A., Kidder, L. E., Mroué, A. H., Pfeiffer, H. P., & Taracchini, A. 2011, PhRvD, 83, 104034
Correia, A. C., Laskar, J., Farago, F., & Boué, G. 2011, CeMDA, 111, 105
Damour, T. 2001, PhRvD, 64, 124013
Damour, T., & Schäfer, G. 1988, NCimB, 101, 127
Davies, M. 2017, in KAVLI Summer Program in Astrophysics: Astrophysics with gravitational wave detections (Copenhagen: Niels Bohr Institute), www.astro.lu.se/~melvyn/mbdcopenhagen2017talk.pdf
De Mink, S. E., & Mandel, I. 2016, MNRAS, 460, 3545
Dominik, M., Belczynski, K., Fryer, C., et al. 2012, ApJ, 759, 52
Dominik, M., Belczynski, K., Fryer, C., et al. 2013, ApJ, 779, 72

Dominik, M., Berti, E., O'Shaughnessy, R., et al. 2015, ApJ, 806, 263
Downing, J. M. B., Benacquista, M. J., Giersz, M., & Spurzem, R. 2010, MNRAS, 407, 1946
Downing, J. M. B., Benacquista, M. J., Giersz, M., & Spurzem, R. 2011, MNRAS, 416, 133
Dvorkin, I., Silk, J., Vangioni, E., Petitjean, P., & Olive, K. A. 2015, MNRAS, 452, L36
Eggleton, P., & Kiseleva-Eggleton, L. 2001, ApJ, 562, 1012
Fabrycky, D., & Tremaine, S. 2007, ApJ, 669, 1298
Farr, B., Holz, D. E., & Farr, W. M. 2018, ApJL, 854, L9
Farr, W. M., Stevenson, S., Miller, M. C., et al. 2017, Natur, 548, 426
Ford, E. B., Kozinsky, B., & Rasio, F. A. 2000, ApJ, 535, 385
Fryer, C. L., Belczynski, K., Wiktorowicz, G., et al. 2012, ApJ, 749, 91
Fryer, C. L., & Kalogera, V. 2001, ApJ, 554, 548
Gerosa, D., Kesden, M., Berti, E., O'Shaughnessy, R., & Sperhake, U. 2013, PhRvD, 87, 104028
Gerosa, D., O'Shaughnessy, R., Kesden, M., Berti, E., & Sperhake, U. 2014, PhRvD, 89, 124025
Giesler, M., Clausen, D., & Ott, C. D. 2018, MNRAS, 477, 1853
Harrington, R. S. 1968, AJ, 73, 190
Hoang, B.-M., Naoz, S., Kocsis, B., Rasio, F. A., & Dosopoulou, F. 2018, ApJ, 856, 140
Hurley, J. R., Pols, O. R., & Tout, C. A. 2000, MNRAS, 315, 543
Hurley, J. R., Tout, C. A., & Pols, O. R. 2002, MNRAS, 329, 897
Kalogera, V. 2000, ApJ, 541, 319
Kozai, Y. 1962, ApJ, 67, 591
Kroupa, P. 2001, MNRAS, 322, 231
Leigh, N. W. C., Geller, A. M., McKernan, B., et al. 2018, MNRAS, 474, 5672
Lidov, M. 1962, P&SS, 9, 719
Liu, B., & Lai, D. 2017, ApJL, 846, L11
Liu, B., & Lai, D. 2018, arXiv:1805.03202
Liu, B., Muñoz, D. J., & Lai, D. 2015, MNRAS, 447, 747
Madau, P., & Dickinson, M. 2014, ARA&A, 52, 415
Mandel, I., & De Mink, S. E. 2016, MNRAS, 458, 2634
Marchant, P., Langer, N., Podsiadlowski, P., Tauris, T. M., & Moriya, T. J. 2016, A&A, 588, A50
Mardling, R. A., & Aarseth, S. J. 2001, MNRAS, 321, 398
Merritt, D. 2013, Dynamics and Evolution of Galactic Nuclei (Princeton, NJ: Princeton Univ. Press)
Miller, M. C., & Lauburg, V. M. 2009, ApJ, 692, 917
Moody, K., & Sigurdsson, S. 2009, ApJ, 690, 1370
Naoz, S. 2016, ARA&A, 54, 441
Naoz, S., Farr, W. M., Lithwick, Y., Rasio, F. A., & Teyssandier, J. 2011, Natur, 473, 187

Naoz, S., Farr, W. M., Lithwick, Y., Rasio, F. A., & Teyssandier, J. 2013, MNRAS, 431, 2155
O'Leary, R., O'Shaughnessy, R., & Rasio, F. 2007, PhRvD, 76, 061504
O'Leary, R. M., Kocsis, B., & Loeb, A. 2009, MNRAS, 395, 2127
O'Leary, R. M., Rasio, F. A., Fregeau, J. M., Ivanova, N., & O'Shaughnessy, R. 2006, ApJ, 637, 937
Peters, P. 1964, PhRv, 136, B1224
Petrovich, C. 2015, ApJ, 799, 27
Petrovich, C., & Antonini, F. 2017, ApJ, 846, 146
Podsiadlowski, P., Rappaport, S., & Han, Z. 2003, MNRAS, 341, 385
Portegies Zwart, S. F., & McMillan, S. L. W. 2000, ApJ, 528, 17
Pürrer, M., Hannam, M., & Ohme, F. 2016, PhRvD, 93, 084042
Repetto, S., & Nelemans, G. 2015, MNRAS, 453, 3341
Rodriguez, C. L., Amaro-Seoane, P., Chatterjee, S., & Rasio, F. A. 2018, PhRvL, 120, 151101
Rodriguez, C. L., Chatterjee, S., & Rasio, F. A. 2016a, PhRvD, 93, 084029
Rodriguez, C. L., Haster, C.-J., Chatterjee, S., Kalogera, V., & Rasio, F. A. 2016b, ApJL, 824, L8
Rodriguez, C. L., Morscher, M., Pattabiraman, B., et al. 2015, PhRvL, 115, 051101
Rodriguez, C. L., Zevin, M., Pankow, C., Kalogera, V., & Rasio, F. A. 2016c, ApJL, 832, L2
Sadowski, A., Belczynski, K., Bulik, T., et al. 2008, ApJ, 676, 1162
Sana, H., de Mink, S. E., de Koter, A., et al. 2012, Sci, 337, 444
Sana, H., Le Bouquin, J. B., Lacour, S., et al. 2014, ApJS, 215, 15
Schnittman, J. D. 2004, PhRvD, 70, 124020
Silsbee, K., & Tremaine, S. 2017, ApJ, 836, 39
Stone, N. C., Metzger, B. D., & Haiman, Z. 2017, MNRAS, 464, 946
Storch, N. I., Anderson, K. R., & Lai, D. 2014, Sci, 345, 1317
Storch, N. I., & Lai, D. 2015, MNRAS, 448, 1821
Tanikawa, A. 2013, MNRAS, 435, 1358
Toonen, S., Hamers, A., & Zwart, S. P. 2016, ComAC, 3, 6
Tremaine, S., Touma, J., & Namouni, F. 2009, ApJ, 137, 3706
Tremaine, S., & Yavetz, T. D. 2014, AmJPh, 82, 769
Trifirò, D., O'Shaughnessy, R., Gerosa, D., et al. 2016, PhRvD, 93, 044071
VanLandingham, J. H., Miller, M. C., Hamilton, D. P., & Richardson, D. C. 2016, ApJ, 828, 77
Vink, J. S., de Koter, A., & Lamers, H. J. G. L. M. 2001, A&A, 369, 574
Vitale, S., Lynch, R., Sturani, R., & Graff, P. 2017, CQGra, 34, 03LT01
Vitale, S., Lynch, R., Veitch, J., Raymond, V., & Sturani, R. 2014, PhRvD, 112, 251101
Voss, R., & Tauris, T. M. 2003, MNRAS, 342, 1169
Ziosi, B. M., Mapelli, M., Branchesi, M., & Tormen, G. 2014, MNRAS, 441, 3703